

ENVIRONMENTAL EFFECTS ON THE STAR FORMATION ACTIVITY AT $Z \sim 0.9$ IN THE COSMOS FIELD*

M. KAJISAWA^{1,2}, Y. SHIOYA¹, Y. AIDA², Y. IDEUE², Y. TANIGUCHI¹, T. NAGAO^{1,3,4}, T. MURAYAMA⁵, K. MATSUBAYASHI¹,
L. RIGUCCINI^{1,6}

Draft version December 2, 2017

ABSTRACT

We investigated the fraction of [O II] emitters in galaxies at $z \sim 0.9$ as a function of the local galaxy density in the Hubble Space Telescope (HST) COSMOS 2 square degree field. [O II] emitters are selected by the narrow-band excess technique with the NB711-band imaging data taken with Suprime-Cam on the Subaru telescope. We carefully selected 614 photo- z selected galaxies with $M_{U3500} < -19.31$ at $z = 0.901 - 0.920$, which includes 195 [O II] emitters, to directly compare results with our previous study at $z \sim 1.2$. We found that the fraction is almost constant at $0.3 \text{ Mpc}^{-2} < \Sigma_{10\text{th}} < 10 \text{ Mpc}^{-2}$. We also checked the fraction of galaxies with blue rest-frame colors of $NUV - R < 2$ in our photo- z selected sample, and found that the fraction of blue galaxies does not significantly depend on the local density. On the other hand, the semi-analytic model of galaxy formation predicted that the fraction of star-forming galaxies at $z \sim 0.9$ decreases with increasing the projected galaxy density even if the effects of the projection and the photo- z error in our analysis were taken into account. The fraction of [O II] emitters decreases from $\sim 60\%$ at $z \sim 1.2$ to $\sim 30\%$ at $z \sim 0.9$ independent of the galaxy environment. The decrease of the [O II] emitter fraction could be explained mainly by the rapid decrease of the star formation activity in the universe from $z \sim 1.2$ to $z \sim 0.9$.

Subject headings: galaxies: environment — galaxies: evolution — galaxies: star formation

1. INTRODUCTION

It is known that star formation activity in galaxies strongly depends on environment in the present universe. The high-density regions such as clusters of galaxies are dominated by passively evolving early-type galaxies, while there are many star-forming late-type galaxies in field (low-density) environments (e.g., Dressler 1980; Goto et al. 2003; Bamford et al. 2009). The fraction of star-forming galaxies systematically decreases with in-

creasing local galaxy density (e.g., Gómez et al. 2003; Balogh et al. 2004; Kauffmann et al. 2004; Tanaka et al. 2004). From these findings, it is considered that the star formation history of galaxies in general depends on environment.

In order to understand how the star formation history of galaxies depends on environment, it is important to investigate the star formation activity of galaxies as a function of environment in the early universe. Several such environmental studies have been carried out at $z > 1$, when the cosmic star formation rate density reached its peak. Hayashi et al. (2010) studied the fraction of narrow-band selected [O II] emitters as a function of the local galaxy density around a cluster at $z \sim 1.5$, and found that the fraction of such star-forming galaxies is nearly independent of the local density, and does not decrease even in the core of the cluster. Tran et al. (2010) also found that the fraction of actively star-forming galaxies with bright IR luminosity slightly increases with the local galaxy density in a cluster at $z = 1.62$. Ideue et al. (2009) similarly investigated the fraction of [O II] emitters in more general environments at $z \sim 1.2$, and found that the fraction is almost constant from low-density to medium-density environments. These results suggest that the relation between the star formation activity and the galaxy environment changed between $z > 1$ and $z \sim 0$. Since the cosmic star formation rate (SFR) density decreases from $z \sim 1$ to the present by about an order of magnitude (e.g., Hopkins & Beacom 2006; Shioya et al. 2008; Westra et al. 2010), the change of the environmental dependence of the star formation activity might be directly related with the decrease of the global SFR density in the universe. Therefore, it is interesting to investigate the star formation activity as a function of environment in detail at $z \sim 1$, when the cosmic SFR density started

* Based on observations with the NASA/ESA *Hubble Space Telescope*, obtained at the Space Telescope Science Institute, which is operated by AURA Inc, under NASA contract NAS 5-26555. Also based on observations made with the Spitzer Space Telescope, which is operated by the Jet Propulsion Laboratory, California Institute of Technology, under NASA contract 1407. Also based on data collected at; the Subaru Telescope, which is operated by the National Astronomical Observatory of Japan; the XMM-Newton, an ESA science mission with instruments and contributions directly funded by ESA Member States and NASA; the European Southern Observatory under Large Program 175.A-0839, Chile; Kitt Peak National Observatory, Cerro Tololo Inter-American Observatory and the National Optical Astronomy Observatory, which are operated by the Association of Universities for Research in Astronomy, Inc. (AURA) under cooperative agreement with the National Science Foundation; and the Canada-France-Hawaii Telescope with MegaPrime/MegaCam operated as a joint project by the CFHT Corporation, CEA/DAPNIA, the NRC and CADC of Canada, the CNRS of France, TERAPIX and the Univ. of Hawaii.

¹ Research Center for Space and Cosmic Evolution, Ehime University, Bunkyo-cho, Matsuyama 790-8577, Japan *e-mail kajisawa@cosmos.phys.sci.ehime-u.ac.jp*

² Graduate School of Science and Engineering, Ehime University, Bunkyo-cho, Matsuyama 790-8577, Japan

³ The Hakubi Project, Kyoto University, Yoshida-Ushinomiya-cho, Sakyo-ku, Kyoto 606-8302, Japan

⁴ Department of Astronomy, Kyoto University, Kitashirakawa-Oiwake-cho, Sakyo-ku, Kyoto 606-8502, Japan

⁵ Astronomical Institute, Graduate School of Science, Tohoku University, Aramaki, Aoba, Sendai 980-8578, Japan

⁶ NASA Ames Research Center, Moffett Field, CA 94035

to decrease.

At $z \sim 1$, several studies in general environments claimed that the average star formation rate of galaxies increases with the local galaxy density (e.g., Elbaz et al. 2007; Cooper et al. 2008), while some studies around clusters of galaxies reported that the fraction of star-forming galaxies decreases with the local density (e.g., Poggianti et al. 2008; Patel et al. 2009; Koyama et al. 2010; Patel et al. 2011). Recently, Sobral et al. (2011) carried out a wide-field near-infrared narrow-band survey in the COSMOS and UKIDSS UDS fields. They found that the fraction of narrow-band selected H α emitters is nearly constant or slightly increases with the local galaxy density from low-density to medium-density environments, and then the fraction decreases towards the highest-density regions such as rich clusters, which is consistent with previous studies both in general fields and clusters regions. Such somewhat complicated environmental dependence of the star formation activity might be considered to be intermediate between those at $z > 1$ and at the present.

The next important step is to investigate the evolution of the star formation activity as a function of environment by directly comparing those in different epochs. For example, Elbaz et al. (2007) and Cooper et al. (2008) made comparisons between $z \sim 1$ and $z \sim 0$ in general fields, while Poggianti et al. (2008) compared the results in groups and clusters at $z = 0.4\text{--}0.8$ with those at $z \sim 0$. In this paper, we focus on the evolution between $z \sim 1.2$ and $z \sim 0.9$, when the cosmic SFR density began to decrease. Using the optical narrow-band imaging data in the COSMOS survey (Scoville et al. 2007) obtained with Suprime-Cam on the Subaru Telescope, we investigated the fraction of narrow-band selected [O II] emitters in galaxies at $z \sim 0.9$ as a function of the local galaxy density. The combination of the wide area of the COSMOS survey and the [O II] emitter selection allows us to construct a large sample of star-forming galaxies with a secure redshift identification. By carefully choosing the selection criteria for our sample and adopting the same method for the estimate of the local galaxy density as our previous study at $z \sim 1.2$ in the COSMOS field (Ideue et al. 2009), we directly compare the star formation activities as a function of environment between $z \sim 0.9$ and $z \sim 1.2$. Section 2 describes the data and the methods for the sample selection and the environment estimate. In Section 3, we show the fraction of [O II] emitters in galaxies at $z \sim 0.9$ as a function of the environment and compare it with that at $z \sim 1.2$, and then check the robustness of the results. In Section 4, we compare our results with previous studies, and then discuss the evolution of the fraction in the redshift interval and its relation to the decrease of the star formation activity in the universe.

Throughout this paper, magnitudes are given in the AB system. We adopt a flat universe with $\Omega_{\text{matter}} = 0.3$, $\Omega_{\Lambda} = 0.7$, and $H_0 = 70 \text{ km s}^{-1} \text{ Mpc}^{-1}$.

2. SAMPLE AND ANALYSIS

2.1. Samples

In this study, we use a sample of galaxies with photometric redshifts of $z = 0.901\text{--}0.920$ from the COSMOS photometric redshift catalog (Ilbert et al. 2009). We can

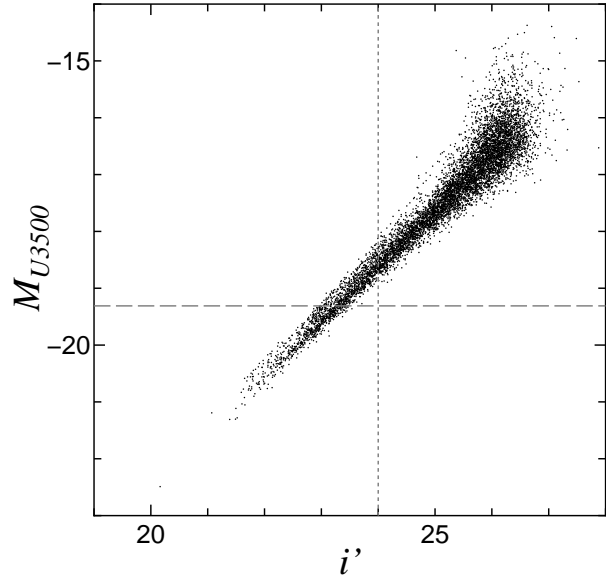


FIG. 1.— M_{U3500} vs. i' for galaxies at $0.901 \leq z_{\text{phot}} \leq 0.920$ from the COSMOS photometric redshift catalog. Horizontal dashed line and vertical dotted line show $M_{U3500} = -19.31$ and $i' = 24.0$, respectively. All galaxies with $M_{U3500} < -19.31$ satisfy $i' < 24.0$.

select [O II] emitters using the NB711 narrow-band data for the redshift interval. In order to directly compare with our previous results at $z \sim 1.2$ (Ideue et al. 2009, hereafter I09), we need to match the magnitude limit of the sample to that at $z \sim 1.2$. In I09, we used the sample of galaxies with $i' < 24$ at $z \sim 1.2$, which corresponds to the rest-frame 3500 Å absolute magnitude of $M_{U3500} < -19.71$. Therefore we constructed a sample of galaxies with $M_{U3500} < -19.71$ at $z = 0.901\text{--}0.920$ (hereafter Sample A). The rest-frame 3500 Å absolute magnitude was calculated from the best-fit SED template derived in the photo- z calculation (Ilbert et al. 2009) for each galaxy.

In addition to the Sample A, we also construct another sample of galaxies at $z = 0.901\text{--}0.920$ using the different magnitude limit, for which the luminosity evolution at the rest-frame 3500 Å between $z \sim 1.2$ and $z \sim 0.9$ is taken into account. In order to measure the strength of the luminosity evolution, we derived the rest-frame 3500 Å luminosity functions (LFs) for the $z \sim 0.9$ and $z \sim 1.2$ samples, and fitted these LFs with the Schechter function. The estimated Schechter parameters are $M_{\star} = -19.55$ and $\log \phi_{\star} = -2.01$ for the $z \sim 0.9$ sample and $M_{\star} = -19.95$ and $\log \phi_{\star} = -1.94$ for the $z \sim 1.2$ sample. The faint-end slope was fixed to $\alpha = -1.0$ in the fitting for the both redshifts. Therefore we assumed that galaxies become fainter by 0.4 mag at the rest-frame 3500 Å from $z \sim 1.2$ to $z \sim 0.9$, and used $-19.71 + 0.4 = -19.31$ as another magnitude limit. The sample of galaxies with $M_{U3500} < -19.31$ at $z = 0.901\text{--}0.920$ is referred to as Sample B.

For the redshift range, we can almost completely sample galaxies even with $M_{U3500} < -19.31$ (Figure 1). All galaxies in the samples have $i' < 24$, and the photometric redshift accuracy is the same as in our previous study at $z \sim 1.2$. The numbers of galaxies in the samples are 373 for the Sample A and 733 for the Sample B. The effective

survey area is 5540 arcmin^2 and the redshift interval of $z = 0.901 - 0.920$ corresponds to the co-moving depth of 50 Mpc. Then our effective survey volume is $2.28 \times 10^5 \text{ Mpc}^3$ given the assumed cosmology.

2.2. [O II] Emitter Selection

We select [O II] emitters from the samples mentioned above as star-forming galaxies using the narrow-band excess technique. In order to select the [O II] emitter, we use the r' , i' , and NB711 bands photometry from the COSMOS photometric catalog (Capak et al. 2007). NB711 is a narrow band with a central wavelength of 7119.6 \AA and a full width at half maximum of 72.5 \AA , which covers the redshifted [O II] $\lambda\lambda 3727$ emission lines for galaxies at $z = 0.901 - 0.920$. We used the $3''$ diameter aperture magnitudes in three bands. We adopted the correction for the photometric zero point presented by Ilbert et al. (2009), which is calculated by comparing the observed multi broad-band photometry for galaxies with spectroscopic identification with the best-fit model templates. The zero-point corrections are 0.003, 0.019, and 0.014 mag for r' , i' , and NB711 bands, respectively. The limiting magnitudes are $r'_{\text{lim}} = 26.6$, $i'_{\text{lim}} = 26.1$, and $\text{NB711}_{\text{lim}} = 24.6$, for a 3σ detection on a $3'' \phi$ diameter aperture. It is noted that we use the CFHT i^* -band magnitude instead of the Subaru/Suprime-Cam i' -band one for galaxies brighter than $i' = 21$ because such bright galaxies appear to be affected by the saturation effect in the Suprime-Cam data. Details of the imaging data and the photometry are given in Taniguchi et al. (2007) and Capak et al. (2007).

In order to select NB711-band excess objects, we calculated a continuum magnitude at the wavelength of NB711 from r and i -bands magnitudes as $f_{ri} = 0.32f_{r'} + 0.68f_{i'}$, where $f_{r'}$ and $f_{i'}$ are the r' and i' flux densities, respectively. Its 3σ limiting magnitude is $ri \simeq 26.5$ in a $3'' \phi$ aperture. For the bright galaxies with $i' < 21$, the ri continuum is calculated as $f_{ri} = 0.32f_{r'} + 0.68f_{i^*}$, where f_{i^*} is the CFHT i^* flux density.

Then, we select NB711-band excess objects using the following criteria:

$$ri - \text{NB711} \geq 0.285 \quad (1)$$

and

$$ri - \text{NB711} > 3\sigma_{ri - \text{NB711}}, \quad (2)$$

where

$$3\sigma_{ri - \text{NB711}} = -2.5 \log \left(1 - \sqrt{(f_{3\sigma_{\text{NB711}}})^2 + (f_{3\sigma_{ri}})^2} / f_{\text{NB711}} \right) \quad (3)$$

The former criterion corresponds to the rest-frame equivalent width $EW_0([\text{O II}]) \geq 12 \text{ \AA}$, which is the same as that in our previous study at $z \sim 1.2$ (I09). Figure 2 shows the color-magnitude distribution for galaxies at $z = 0.901 - 0.920$. Red symbols represent galaxies with $M_{U3500} < -19.71$ (Sample A), and blue ones show galaxies with $-19.71 < M_{U3500} < -19.31$. The narrow and broad-bands data are deep enough to almost completely sample galaxies with $EW_0([\text{O II}]) \geq 12 \text{ \AA}$. Here, we exclude X-ray sources as active galactic nuclei (AGNs) based on the X-ray information given in the COSMOS photo- z catalog (Ilbert et al. 2009). Finally, we select 118 [O II] emitters out of 373 galaxies in the Sample A

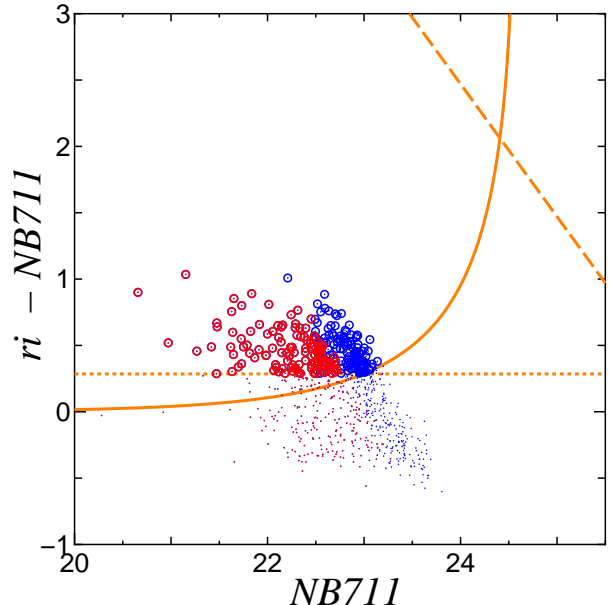


FIG. 2.— $ri - \text{NB711}$ vs. NB711 for galaxies with $M_{U3500} < -19.31$ at $0.901 \leq z_{\text{phot}} \leq 0.920$. Large open circles show objects classified as [O II] emitters. Red symbols show galaxies with $M_{U3500} \leq -19.71$ (the Sample A), while blue symbols represent those with $-19.71 < M_{U3500} < -19.31$ (i.e., red + blue = the Sample B). The dotted line corresponds to the minimum excess of $ri - \text{NB711} = 0.285$, and the solid curve shows the 3σ error of $ri - \text{NB711}$ color. The dashed line represents the 3σ sensitivity limit for ri magnitude.

and 233 [O II] emitters out of 733 galaxies in the Sample B.

We also examine how many AGNs are included in our sample using Spitzer IRAC mid-infrared colors. Lacy et al. (2004) and Stern et al. (2005) pointed out that AGNs can be distinguished from star-forming galaxies using Spitzer IRAC colors, e.g., $[3.6] - [4.5]$. While the ultraviolet to mid-infrared ($\lambda < 5 \mu\text{m}$) continuum of star-forming galaxies is the composite stellar continuum that peaks at $\sim 1.6 \mu\text{m}$, an AGN continuum is well fit by a power law. The infrared colors of AGNs tend to be systematically redder than star-forming galaxies. As in I09, we select objects with a mid-infrared color of $[3.6] - [4.5] > 0$ as AGN. We apply this criterion for the 207 [O II] emitters detected in both 3.6 and $4.5 \mu\text{m}$. We find that 2 out of the 207 [O II] emitters in our sample satisfy this criterion; the fraction of the possible AGNs is $2/207 = 1.0 \%$ at most. Therefore, we consider that the AGN contamination does not affect our discussion below.

2.3. Local Surface Density

As in I09, we use the 10th nearest neighbor method to estimate the local surface density of galaxies as a measurement of the galaxy environment. The projected surface density is calculated as

$$\Sigma_{10\text{th}} = \frac{11}{\pi r^2}, \quad (4)$$

where r is the distance to 10th nearest neighbor. We calculate this distance for galaxies within the redshift $z \pm \sigma_z$ taking account of the error of the photometric

TABLE 1
SUMMARY OF THE SAMPLES

	photometric redshift	limiting magnitude	total number ($\Sigma_{10\text{th}}$ available)	# of [O II] emitters ($\Sigma_{10\text{th}}$ available)
Sample A	0.901–0.920	$M_{U3500} < -19.71$	373 (291)	118 (95)
Sample B	0.901–0.920	$M_{U3500} < -19.31$	733 (614)	233 (195)

redshift ($\sigma_z = 0.023$ at $z \sim 0.9$). The redshift slice of $z \pm \sigma_z$ corresponds to the co-moving depth of 118 Mpc, while that in our previous study at $z \sim 1.2$ is 114 Mpc (I09). Therefore, the co-moving depth for the estimate of the projected surface density in this study is similar with that in I09. We consider that such a small difference in the depth of the redshift slice does not affect our results shown in the next section. We discard the galaxies near the edge of our field of view, i.e., whose r is larger than the distance to the edge of the field. This procedure decreases the numbers of galaxies in our samples to 291 (95 [O II] emitters) for the Sample A and 614 (195 [O II] emitters) for the Sample B. We summarize our samples in Table 1.

3. RESULTS

3.1. Fraction of [O II] emitters at $z \sim 0.9$ as a function of local density

Figure 3 shows the fraction of [O II] emitters in galaxies at $z \sim 0.9$ as a function of the local galaxy density. The results for the Samples A and B are shown as solid circles and open squares, respectively. For comparison, we also show the results for galaxies at $z \sim 1.2$ from I09.

In Figure 3, we cannot find a significant environmental dependence of the fraction of [O II] emitters in the both Samples A and B. The fraction of [O II] emitters is nearly constant (~ 0.3) for between $\Sigma_{10\text{th}} \sim 0.3 \text{ Mpc}^{-2}$ and $\sim 10 \text{ Mpc}^{-2}$. Even if we take the effect of luminosity evolution of galaxies into account, the flat distribution holds. The fraction of [O II] emitters at $z \sim 1.2$ also shows no significant environmental dependence, but the fraction is ~ 0.6 over a wide range of the local density, which is significantly higher than that at $z \sim 0.9$. The fraction of [O II] emitters decreases from ~ 0.6 to ~ 0.3 between $z \sim 1.2$ and $z \sim 0.9$ in all environments we investigated.

We check the effects of the projection and the photometric redshift error on these results, in the following sections.

3.2. Fraction of galaxies with blue $NUV - R$ color

In the analysis of the previous section, we mainly used the sample of galaxies with $0.901 \leq z_{\text{phot}} \leq 0.920$ (i.e., $\Delta z = 0.019$) to select [O II] emitters as the star-forming population, while the local galaxy density are calculated with galaxies within a redshift slice of $z \pm \sigma_z$ (i.e., $\Delta z = 0.046$) taking account of the photo- z error. So the density measurement includes galaxies outside the main sample. Furthermore, as we show in Section 3.4, [O II] emitters selected by the NB711-band excess tend to have higher photo- z accuracy than the other galaxies without the narrow-band excess.

In order to check whether they affect the environmental dependence of the fraction of star-forming galaxies, we selected star-forming galaxies by the rest-frame $NUV - R$

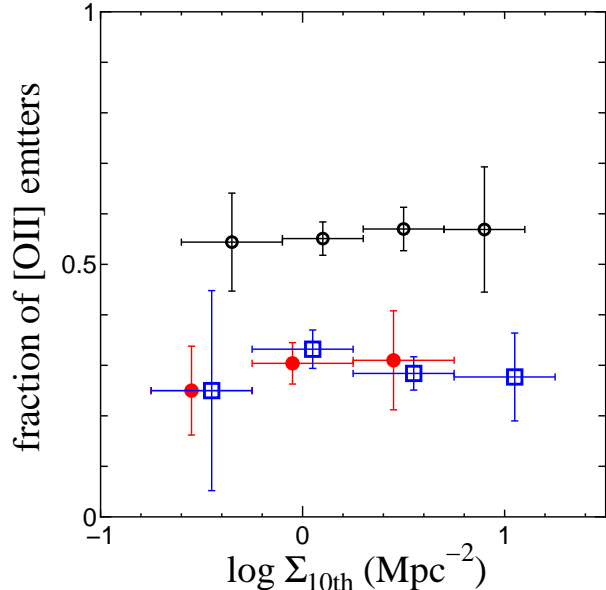


FIG. 3.— Fraction of [O II] emitters as a function of the galaxy local density. Filled circles show the result for the Sample A and open squares show that for the Sample B. Small open circles represent the result at $z \sim 1.2$ updated from Ideue et al. (2009) with the newest version of the COSMOS photometric redshift catalog.

color estimated from the COSMOS multi-band photometric data instead of $EW_0([\text{O II}])$. The $EW_0([\text{O II}])$ is the ratio of the line luminosity $L([\text{O II}])$ and the continuum luminosity at the rest-frame 3727\AA . While $L([\text{O II}])$ mainly depend on SFR, the continuum luminosity at 3727\AA depends on both SFR and stellar mass. Therefore we consider that the rest-frame $NUV - R$ color is more suitable for a substitute for $EW_0([\text{O II}])$ than the simple rest-frame UV luminosity. If we ignore the effect of the dust reddening, star-forming galaxies with large $EW_0([\text{O II}])$ are expected to have blue $NUV - R$ colors. Since the rest-frame $NUV - R$ selection is not limited to the narrow redshift range of $z_{\text{phot}} = 0.901-0.920$, we can estimate the fraction of blue star-forming galaxies and the local galaxy density with the same sample within a redshift slice of $\Delta z = 0.046$.

Figure 4 shows the two color diagram of $NUV - R$ vs. $R - J$ for galaxies at $0.901 \leq z_{\text{phot}} \leq 0.920$. It is seen that [O II] emitters tend to show blue $NUV - R$ colors as expected. Since more than 90% of [O II] emitters have $NUV - R < 2$, we use $NUV - R < 2$ as the selection criterion for blue star-forming galaxies. The average fraction of galaxies with $NUV - R < 2$ is 47% in the Sample A, which is slightly larger than that of [O II] emitters. Figure 5 shows the fraction of galaxies with $NUV - R < 2$ in the Sample A as a function of the local galaxy density. We first used galaxies at $0.901 \leq z_{\text{phot}} \leq 0.920$ as the main sample and measured

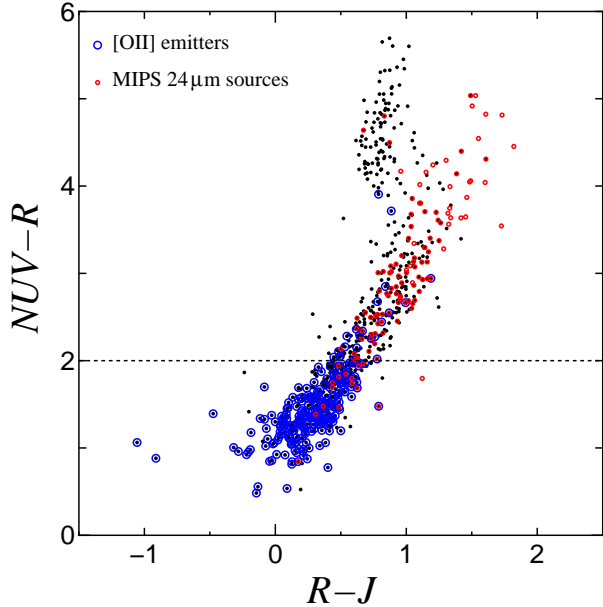


FIG. 4.— The rest-frame $NUV - R$ vs. $R - J$ diagram for the Sample B ($M_{U3500} < -19.31$). Blue circles show [O II] emitters selected by the NB711-band excess. Red circles represent bright Spitzer/MIPS $24\mu\text{m}$ sources with $f_{24\mu\text{m}} \gtrsim 150\text{--}200 \mu\text{Jy}$ at $z_{\text{phot}} = 0.901\text{--}0.920$, which include those objects with $M_{U3500} > -19.31$.

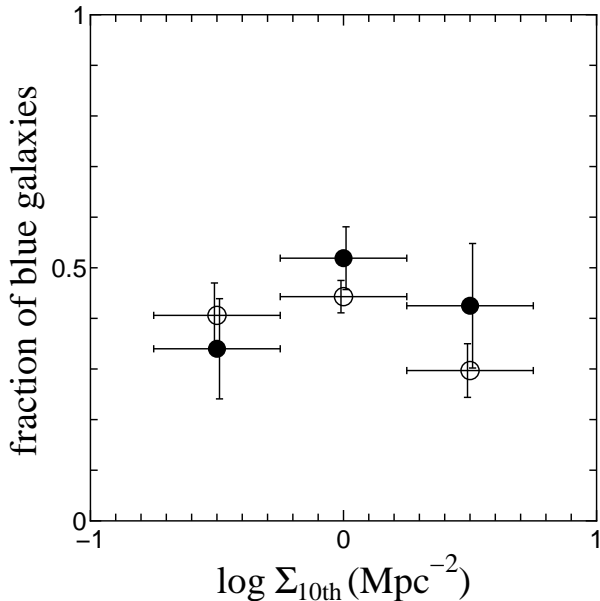


FIG. 5.— Fraction of blue galaxies with the rest $NUV - R < 2$ as a function of the local galaxy density. Solid circles show the result for galaxies with $M_{U3500} < -19.71$ at $0.901 \leq z_{\text{phot}} \leq 0.920$. The local density for each sample is measured with galaxies within a redshift slice of $z \pm 0.023$ centered on its redshift, as in Figure 3. On the other hand, open circles show the case that both the fraction of blue galaxies and the local galaxy density are measured from the same galaxy sample at $0.91 - 0.023 \leq z_{\text{phot}} \leq 0.91 + 0.023$.

the local density for each sample galaxy by using galaxies within a redshift slice of $z \pm \sigma_z$ centered on its redshift, as in the case of [O II] emitters (solid circles in Figure 5). Then we estimated both the fraction of blue galaxies

and the local galaxy density from the same galaxies at $0.91 - 0.023 \leq z_{\text{phot}} \leq 0.91 + 0.023$ (open circles in the figure). The fractions of galaxies with $NUV - R < 2$ in the both cases agree within the uncertainty at each density. The fraction does not significantly depend on the local density in the both cases, although the fraction could be slightly smaller at the highest density bin in the latter case. If we use the Sample B instead of the Sample A, we obtain the similar results. Therefore we consider that the difference in the redshift range between the main sample and the sample used for the density measurement does not significantly affect our results.

3.3. Comparison with the semi-analytic model

Although more than 30 photometric bands of the COSMOS data set provide the very accurate photometric redshift, the error of $\sigma_z = 0.023$ at $z \sim 0.9$ corresponds to relatively large physical scale of ~ 30 Mpc. The effects of the projection over the redshift slice of $z \pm \sigma_z$ (~ 60 Mpc width in physical scale) and the photo- z error could wash out structures or make spurious overdensities.

In order to check these effects, we use a mock galaxy catalogue from the publicly available semi-analytic model by Font et al. (2008). This model is based on the Millennium Simulation of the growth of dark matter structure in a Λ cold dark matter cosmology (Springel et al. 2005) and is a minor revision of the model by Bower et al. (2006). We sampled model galaxies with $M_U < -19.71$ and $M_U < -19.31$ from a snapshot at $z \sim 0.9$, and then calculated the local galaxy densities with three ways; 1) 3-dimensional density based on the 10th nearest neighbor (i.e., true density), 2) 2-dimensional projected density based on the 10th nearest neighbor which is calculated from samples within a slice of 60 Mpc in physical scale, 3) the same as 2) but calculated from samples within a slice of 60 Mpc after galaxies are randomly shifted along the depth direction of the slice with a offset of the Gaussian distribution with $\sigma = 30$ Mpc in order to take the photometric redshift error of the observed sample into account. We can check the projection effect by comparing 1) and 2), and see the effect of the photometric redshift uncertainty from 3). Figure 6 shows the comparison between 1) and 2) (left panel) and that between 1) and 3) (right panel) for the sample with $M_U < -19.71$. It is seen from the left panel that there is a clear correlation with a scatter of $\sigma \sim 0.3$ dex between the true density and 2-dimensional projected density. Even if the random offsets by the photometric redshift error are added (the right panel), there remains the correlation between the true and projected densities although both high and low density regions seem to be smeared out in some degree and the correlation becomes weaker. The results for the sample with $M_U < -19.31$ are the same except that the both true and projected densities become slightly larger simply because of the increase of the number of galaxies in the sample. We confirmed that these results do not depend on a choice of the direction of the slice in the simulation box.

We also checked the environmental dependence of the fraction of [O II] emitters in the simulation by calculating $EW_0([\text{O II}])$ of model galaxies from their $L([\text{O II}])$ and M_U in the mock catalogue. Figure 7 shows the fraction of galaxies with $EW_0([\text{O II}]) > 12 \text{ \AA}$ as a function of the 3-dimensional density (left panel) and the 2-

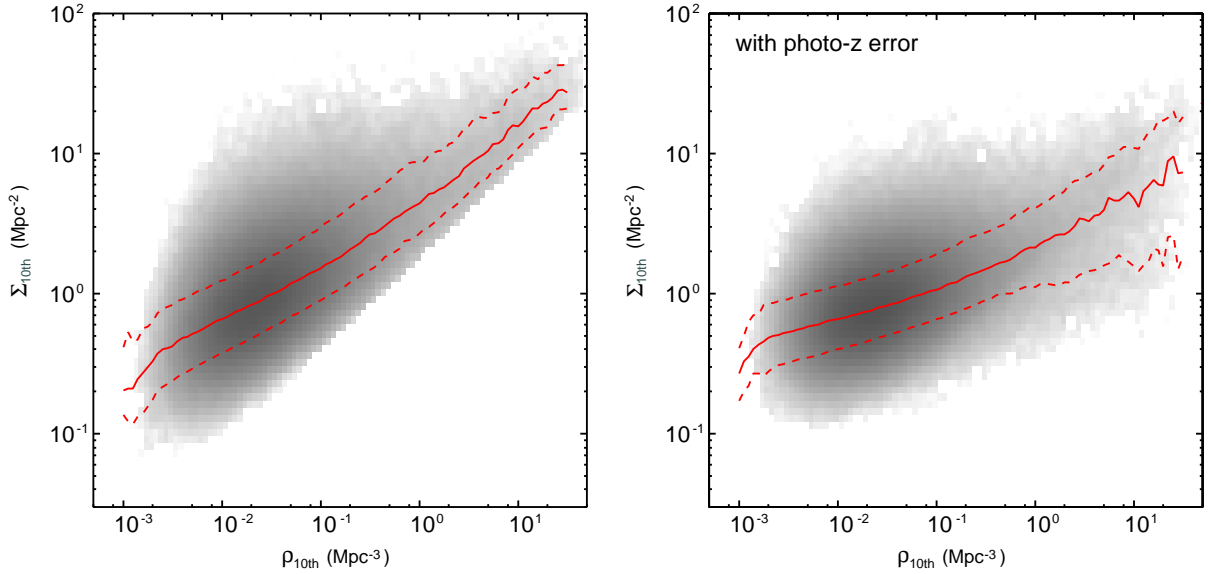


FIG. 6.— **left**) Comparison between the 3-dimensional (true) local galaxy density and the projected 2-dimensional density for ~ 550000 mock galaxies with $M_U < -19.71$ at $z \sim 0.9$ in the semi-analytic model by Font et al. (2008). The both densities are estimated by the 10th nearest neighbor method. The 2-dimensional projected density is calculated from model galaxies within a slice of 60 Mpc in physical scale, which corresponds to $\Delta z = 0.046$ at $z \sim 0.9$. Solid line shows the median value of the projected density as a function of the 3-dimensional density, while dashed lines represent the 16 and 84 percentiles. **right**) The same as the left panel but the projected density is calculated from model galaxies within a slice of 60 Mpc after galaxies are randomly shifted with a offset of the Gaussian distribution with $\sigma = 30$ Mpc in order to take account of the photometric redshift error (see text).

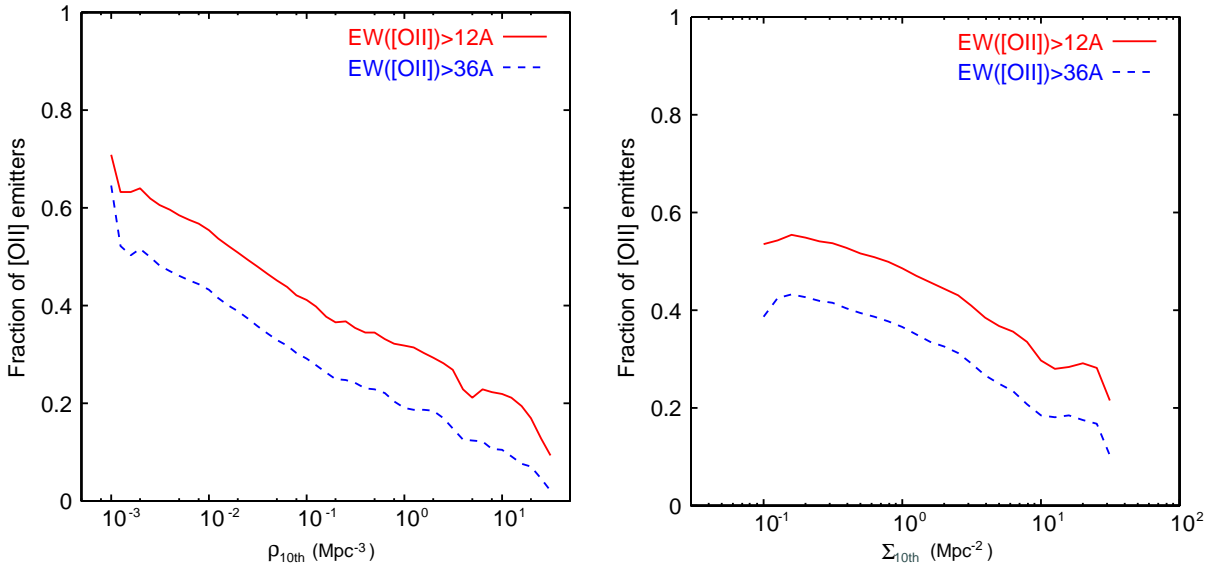


FIG. 7.— **left**) Fraction of [O II] emitters in mock galaxies with $M_U < -19.71$ at $z \sim 0.9$ in the semi-analytic model by Font et al. (2008) as a function of the 3-dimensional local galaxy density. Solid line shows the fraction of galaxies with $EW_0([\text{O II}]) > 12 \text{ \AA}$, and dashed line shows that of galaxies with $EW_0([\text{O II}]) > 36 \text{ \AA}$. **right**) The same as the left panel but as a function of the 2-dimensional projected density with the photometric redshift error of $\sigma_z = 0.023$.

dimensional projected density with the photometric redshift error (right panel). Since the overall fraction is slightly larger than the observed fraction of [O II] emitters, we also show the fraction of model galaxies with $EW_0([\text{O II}]) > 36 \text{ \AA}$ for comparison. It is seen from the left panel that the fraction of star-forming galaxies selected by the $EW_0([\text{O II}])$ criteria clearly decreases with the local galaxy density in the semi-analytic model as previous studies have already reported (e.g., Elbaz et al.

2007). Even if we use the projected density with the photometric redshift error, the fraction of [O II] emitters clearly depends on the density, although the environmental dependence of the fraction becomes slightly weaker. This suggests that the effects of the projection and the photometric redshift error in our density measurement do not smear out the relation between the fraction of [O II] emitters and local density. The observed fraction in Figure 3 does not seem to decrease with the local density,

which is different from the semi-analytic model, although the relatively large statistical error in our analysis prevents us from completely rejecting the model.

We note that the above simulation of the fraction of [O II] emitters with the semi-analytic model does not consider the fact that [O II] emitters are selected by the narrow-band excess within a narrower redshift width of $\Delta z = 0.019$. As seen in the previous subsection, however, we obtained the same result (no significant environmental dependence) when we selected galaxies with blue rest-frame $NUV - R$ colors as the star-forming population within the same redshift width of $\Delta z = 0.046$ as in the local density measurement. Therefore, we consider that it does not affect the comparison between our result and the model prediction.

3.4. Incompleteness and contamination due to the photometric redshift error

We here check the incompleteness and contamination due to the photometric redshift error in our sample by using spectroscopic redshifts from the zCOSMOS redshift survey (Lilly et al. 2007; Lilly et al. 2009). Since the NB711 data are used in the photometric redshift measurement (Ilbert et al. 2009), the photometric redshifts of [O II] emitters with the narrow-band excess are expected to be more accurate than the other galaxies without the narrow-band excess (hereafter, non-[O II] emitters) in our sample. Therefore we investigated the incompleteness and contamination for [O II] emitters and non-[O II] emitters separately.

We first examined the spectroscopic redshift distribution for the photo-z selected galaxies with $M_{U3500} < -19.71$ (Sample A) in order to estimate the fraction of the contamination from outside the redshift range into the photo-z selected sample. There are 24 [O II] emitters and 65 non-[O II] emitters with spectroscopic identification in the Sample A, and we can use these galaxies for the purpose. Out of 24 [O II] emitters, 19 have spectroscopic redshifts of $0.901 \leq z_{\text{spec}} \leq 0.920$, and the other 5 objects have spectroscopic redshifts outside of the redshift range (i.e., $z_{\text{spec}} < 0.901$ or $z_{\text{spec}} > 0.920$). If we consider these 5 objects as the contaminants from outside the redshift range, the fraction of the contamination from outside the redshift range is $5/24 = 21\%$. Actually, four of these 5 objects have slightly lower redshifts of $z_{\text{spec}} = 0.893-0.899$, for which the [O II] emission enters into the short-wavelength wing of the NB711 filter, while one object is a [O III] emitter at $z_{\text{spec}} = 0.422$. So if we include four objects with $z_{\text{spec}} = 0.893-0.899$ into the [O II] emitter sample, the contamination rate becomes $1/24 = 4\%$. On the other hand, 39 of 65 non-[O II] emitters in the Sample A lie within $0.901 \leq z_{\text{spec}} \leq 0.920$, and the other 26 objects have spectroscopic redshifts of $z_{\text{spec}} < 0.901$ or $z_{\text{spec}} > 0.920$. Therefore, the contamination rate for non-[O II] emitters is $26/65 = 40\%$.

Next, we checked the photometric redshift distribution of galaxies with $z_{\text{spec}} = 0.901-0.920$ and $M_{U3500} < -19.71$ to estimate the incompleteness due to the photo-z error for the Sample A. From the spectroscopic catalogue, we could use 97 objects with $z_{\text{spec}} = 0.901-0.920$ and $M_{U3500} < -19.71$, and found that 58 out of 97 have photometric redshifts of $0.901 \leq z_{\text{phot}} \leq 0.920$. While these 58 objects are included into our photo-z selected sample, the other 39 objects are missed by the photo-z

selection. Out of 97 objects with $z_{\text{spec}} = 0.901-0.920$, 20 objects shows a significant NB711-band excess and satisfy the criteria for [O II] emitters, and the other 77 objects are non-[O II] emitters. Similarly, out of 58 objects with $z_{\text{spec}} = 0.901-0.920$ and $z_{\text{phot}} = 0.901-0.920$, 19 objects satisfy the criteria for [O II] emitters, and the other 39 objects are non-[O II] emitters. Therefore, for [O II] emitters, 19 out of 20 galaxies with $z_{\text{spec}} = 0.901-0.920$ are selected to the Sample A, and the completeness is $19/20 = 95\%$. On the other hand, 39 out of 77 non-[O II] emitters with $z_{\text{spec}} = 0.901-0.920$ are included into the sample. Therefore the completeness for non-[O II] emitters is $39/77 = 51\%$.

By adopting these contamination and completeness rates, which is estimated from the spectroscopic sample, for all the photo-z selected sample, we examined the effects of the contamination and incompleteness due to the photo-z error on the fraction of [O II] emitters in the photo-z selected sample. Since the contamination and completeness rates for [O II] emitters are 21% and 95%, respectively, we select 95% of the real [O II] emitters and also pick up the contaminants which account for 21% of the observed number. Therefore, the number of [O II] emitters are expected to be overestimated by $\sim 20\%$; i.e., $0.95/(1 - 0.21) \sim 1.20$. Similarly, from the contamination rate of 40% and the completeness of 51%, we can calculate that the observed number of non-[O II] emitters is underestimated by $\sim 15\%$; i.e., $0.51/(1 - 0.40) \sim 0.85$. Since the observed numbers of [O II] emitters and non-[O II] emitters are 95 and 196 respectively, the number of all photo-z selected galaxies is expected to be underestimated by $\sim 6\%$; i.e., $(95 + 196)/(95/1.21 + 196/0.85) \sim 0.94$. As a result, the number of [O II] emitters is overestimated by $\sim 20\%$, while the number of the all photo-z sample is underestimated by $\sim 6\%$. Therefore, the fraction of [O II] emitters could be overestimated by $\sim 28\%$; i.e., $1.20/0.94 = 1.28$. If we do not consider the four [O II] emitters with $z_{\text{spec}} = 0.893-0.899$ as the contaminants, the contamination rate for [O II] emitters decreases from 21% to 4% as mentioned above, and the overestimation of the fraction of [O II] emitters becomes $\sim 5\%$. Since Ideue et al. (2012) estimated that the fraction of [O II] emitters at $z \sim 1.2$ could be overestimated by $\sim 17\%$ due to the photo-z error, the fractions of [O II] emitters at $z \sim 1.2$ and $z \sim 0.9$ might be similarly overestimated.

4. DISCUSSION

4.1. Comparison with other studies

We here compare our results in the COSMOS field with previous studies of the environmental dependence of the star formation activity in galaxies at similar redshifts. Elbaz et al. (2007) investigated the average SFR of galaxies with $M_B < -20$ at $0.8 \leq z \leq 1.2$ as a function of the local galaxy density in the GOODS fields. They found that the average SFR increases with the density and seems to peak around a density of $\sim 2-3 \text{ Mpc}^{-2}$. Our results seem to be consistent with their results in that the fraction of actively star-forming galaxies does not decrease with the local density on average, which is different from the SFR-density relation seen in the present universe and from the predictions by the semi-analytic models of the galaxy formation. However, the

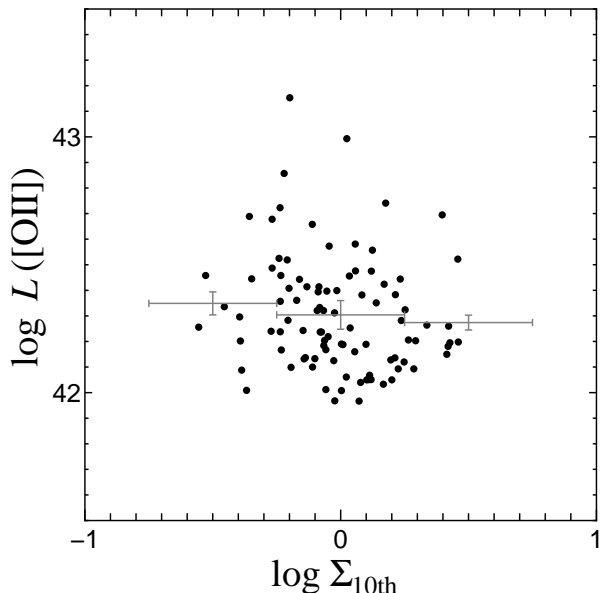


FIG. 8.— [O II] luminosity vs. the local galaxy density for [O II] emitters with $M_{U3500} < -19.71$. The [O II] luminosity is corrected for the dust extinction under the assumption of $A_{H\alpha} = 1$ mag for all [O II] emitters (see Appendix).

fraction of [O II] emitters at $z \sim 0.9$ in the COSMOS field does not significantly depend on the density and does not seem to peak around a density of several Mpc^{-2} . In order to examine the environmental dependence of the average SFR in our sample, we plot $L([\text{O II}])$ of [O II] emitters as a function of the local density in Figure 8. $L([\text{O II}])$ is estimated from the r_i and $NB711$ magnitudes (see Appendix for detail). It is seen that the $L([\text{O II}])$ of [O II] emitters is also independent of the density. Therefore we expect that the average $L([\text{O II}])$ also does not significantly depend on the local density.

A possible origin of the different behaviors in the SFR-density relation between Elbaz et al. (2007) and this study is the effect of the dust extinction. We selected star-forming galaxies with the [O II] emitter selection, while Elbaz et al. (2007) estimated SFRs of galaxies from the Spitzer/MIPS $24 \mu\text{m}$ fluxes. Although we correct $L([\text{O II}])$ for the dust extinction assuming $A_{H\alpha} = 1$ mag, the [O II] emitter selection itself could miss dusty star-forming galaxies. In order to check this, we cross-matched the $24 \mu\text{m}$ source catalogue from the S-COSMOS survey (Sanders et al. 2007) to galaxies at $0.901 \leq z_{\text{phot}} \leq 0.920$ in our sample. The flux limit of the $24 \mu\text{m}$ catalogue is $\sim 150\text{--}200 \mu\text{Jy}$. We plot the $24 \mu\text{m}$ sources as red circles in Figure 4. These bright $24 \mu\text{m}$ sources tend to show red rest-frame $NUV - R$ and $R - J$ colors, and the overlap between these $24 \mu\text{m}$ sources and [O II] emitters is relatively small. Since star-forming galaxies are expected to distribute over a diagonal region from $(R - J \sim 0, NUV - R \sim 1)$ to $(R - J \sim 1.5, NUV - R \sim 4.5)$ (e.g., Bundy et al. 2010), the [O II] selection seems to miss star-forming galaxies with relatively red $NUV - R$ colors such as the bright $24 \mu\text{m}$ sources. We also compare the stellar mass of [O II] emitters with that of these bright $24 \mu\text{m}$ sources in Figure 9. The stellar mass of each galaxy is estimated by fitting the multi-band photometric data

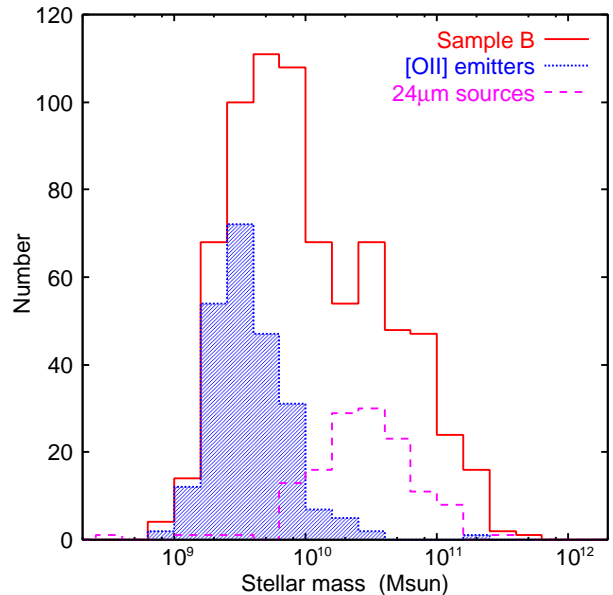


FIG. 9.— Distribution of the stellar mass of galaxies for the Sample B ($M_{U3500} < -19.31$). The solid line shows all galaxies in the Sample B, while the shaded dotted histogram shows [O II] emitters with $M_{U3500} < -19.31$. The dashed histogram represents the bright MIPS $24 \mu\text{m}$ sources with $f_{24 \mu\text{m}} \gtrsim 150\text{--}200 \mu\text{Jy}$.

from UV to MIR wavelength with the population synthesis model by Bruzual & Charlot (2003) (Ilbert et al. 2010). Chabrier (2003)'s IMF is assumed. Figure 9 shows that most of [O II] emitters have relatively low stellar mass of $M_{\text{star}} \lesssim 10^{10} M_{\odot}$, while the all photo- z selected galaxies distribute over $10^9 M_{\odot} \lesssim M_{\text{star}} \lesssim 10^{11} M_{\odot}$. On the other hand, the bright $24 \mu\text{m}$ sources show systematically larger stellar mass of $\sim 10^{10}\text{--}10^{11} M_{\odot}$. The $24 \mu\text{m}$ -selected star-forming galaxies in Elbaz et al. (2007) also distribute over $10^9 M_{\odot} \lesssim M_{\text{star}} \lesssim 10^{11} M_{\odot}$. Therefore the [O II] emitter selection seems to miss massive (dusty) star-forming population. Since star-forming galaxies with $10^{10}\text{--}10^{11} M_{\odot}$ have a large contribution to the cosmic SFR density at $z \sim 1$ (e.g., Kajisawa et al. 2010), these massive star-forming galaxies could significantly contribute the average SFR in each environment. The contribution from these massive galaxies might cause the peak of the average SFR around a local density of $\sim 2\text{--}3 \text{Mpc}^{-2}$ seen in Elbaz et al. (2007). However, we note that the fraction of star-forming galaxies in our sample does not significantly depend on the density, even if we include the bright $24 \mu\text{m}$ sources into the star-forming population.

Another possible origin of the different results is the different scales of the local density measurement. Elbaz et al. (2007) measured the density with a box of $1.5 \text{Mpc} \times 1.5 \text{Mpc} \times 40 \text{Mpc}$ in comoving scale, while we used the 10th nearest neighbor method with galaxies within a comoving depth of 118 Mpc. In the 10th nearest neighbor method, a radius used in the density measurement depends on the local density itself. For example, the local density of $\Sigma_{10\text{th}} = 1 \text{Mpc}^{-2}$ corresponds to a radius of $r_{10\text{th}} \sim 3.6 \text{Mpc}$ in comoving scale ($\sim 1.9 \text{Mpc}$ in physical scale). When the local density is 10Mpc^{-2} , a radius becomes 1.1 Mpc in comoving scale. Since we typically investigate galaxies with $\Sigma_{10\text{th}} \sim 1\text{--}10 \text{Mpc}^{-2}$

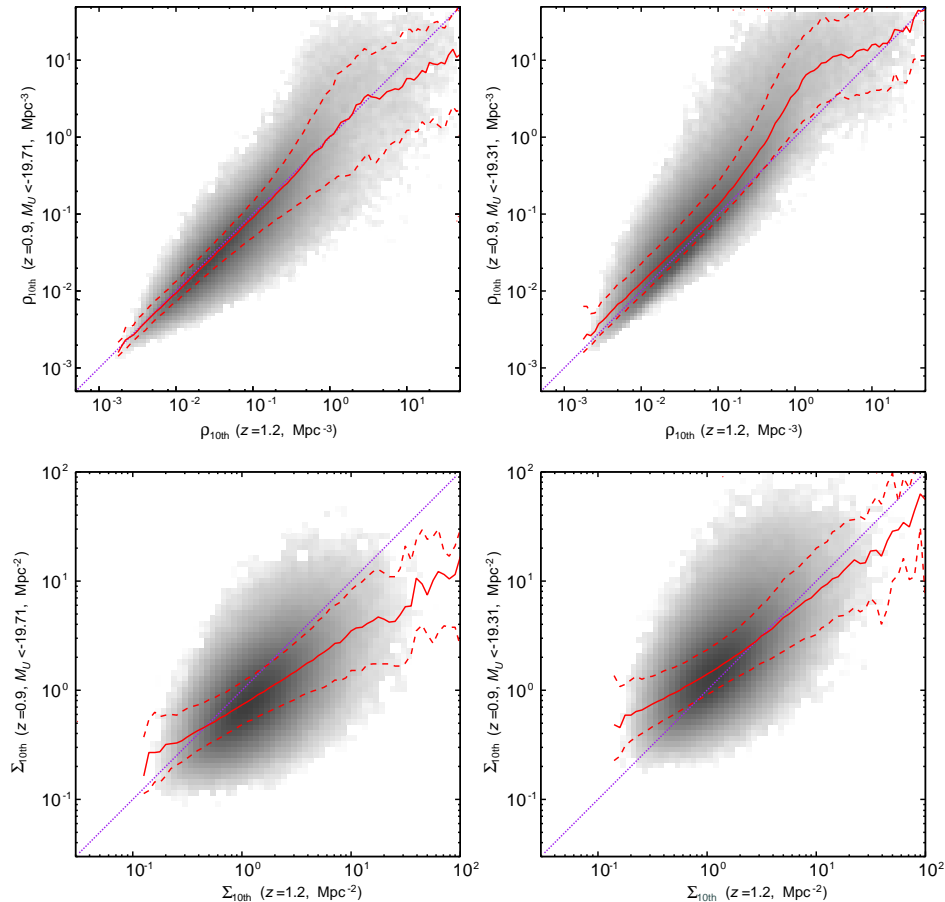


FIG. 10.— Evolution of the local galaxy density between $z \sim 1.2$ and $z \sim 0.9$ for mock galaxies in the semi-analytic model by Font et al. (2008). Top panels show comparisons of the 3-dimensional local densities at the different redshifts for the same model galaxies, while bottom panels show those of the 2-dimensional projected densities with the photometric redshift error. The local density at $z \sim 1.2$ is estimated from galaxies with $M_U < -19.71$. Left panels show the case that the local density at $z \sim 0.9$ is estimated from galaxies with $M_U < -19.71$, while right panels show the results for the density at $z \sim 0.9$ measured from those with $M_U < -19.31$. Solid line shows the median value of the density at $z \sim 0.9$ as a function of the density at $z \sim 1.2$, while dashed lines represent the 16 and 84 percentiles.

(Figure 3), the local density in our analysis is measured with a radius of 1.1–3.6 Mpc, which corresponds to a diameter of 2.2–7.2 Mpc. This scale is larger than that in Elbaz et al. (2007) (1.5 Mpc), especially for low-density environments. The depth of 118 Mpc used in our density measurement is also much larger than 40 Mpc used in Elbaz et al. (2007). For local galaxies, Blanton et al. (2006) pointed out that the environment dependence of the star formation activity in galaxies could vary with the scale used for the density measurement. Elbaz et al. (2007) also discussed that the peak of the average SFR around a density of $\sim 3 \text{ Mpc}^{-2}$ seen in their result could be caused by active star formation in galaxies during group formation at the scale of ~ 1 Mpc. The density measurement in a relatively large scale might smear out such small-scale environmental effect in some degree.

On the other hand, Poggianti et al. (2008) studied the star formation activity of galaxies as a function of the local density mainly in clusters and groups at $z = 0.4$ – 0.8 . They found that the fraction of [O II] emitters in groups or outskirts of clusters is similar with that in field environments at the same redshift, while the fraction decreases toward the highest-density region at the cores of clusters. The weak or no environmental dependence of the fraction of [O II] emitters at the relatively low-

density environment ($\Sigma_c < 15$ – 40 Mpc^{-2}) might be consistent with our results, although the fraction of $\sim 70\%$ in Poggianti et al. (2008) is much higher than that in this study because they selected objects with $EW_0([\text{O II}]) > 3 \text{ \AA}$ as [O II] emitters by using the spectroscopic data. They also pointed out that the average SFR of [O II] emitters has a peak at $\Sigma_c \sim 15$ – 40 Mpc^{-2} , while we found no significant environmental dependence of the [O II] luminosity at the lower density. Patel et al. (2011) similarly studied SFRs of galaxies at $0.6 < z < 0.9$ as a function of local density including the group and cluster environments, and found that both the fraction of star-forming galaxies and the average SFR of star-forming galaxies decrease at densities much higher than the field environments. But we note that their sample is limited to relatively massive galaxies with $M_{\text{star}} > 10^{10.25} M_\odot$, while [O II] emitters in this study tend to have smaller mass of $M_{\text{star}} < 10^{10} M_\odot$ as seen in Figure 9.

Recently, Sobral et al. (2011) investigated the fraction of H α emitters in galaxies with $K < 23$ at $z \sim 0.84$ in the COSMOS and UKIDSS UDS fields (total $\sim 1.3 \text{ deg}^2$), using a narrow-band observations at $1.211 \mu\text{m}$. They also used the 10th nearest neighbor method to measure the local density and studied the environmental dependence of the fraction of star-forming galaxies. They found that

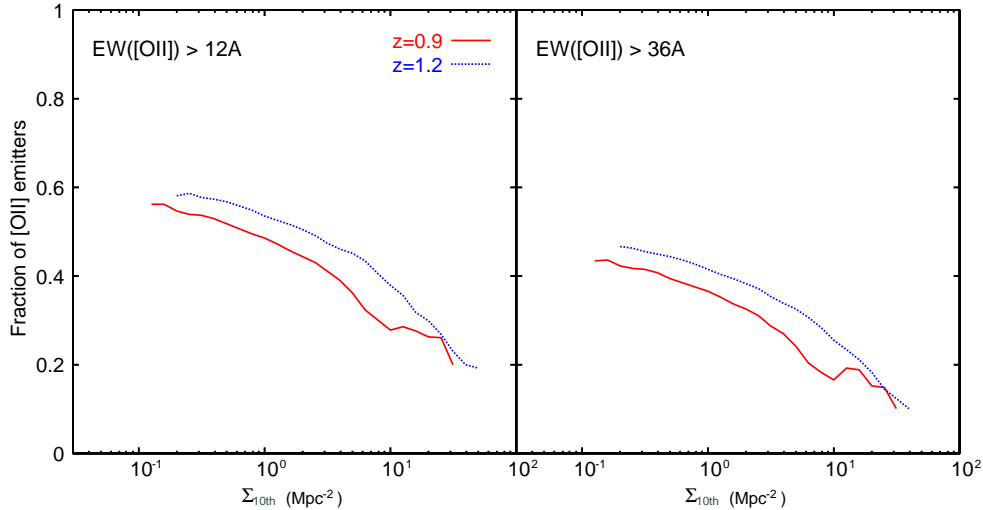


FIG. 11.— Evolution of the fraction of [O II] emitters between $z \sim 1.2$ and $z \sim 0.9$ for mock galaxies with $M_U < -19.71$ in the semi-analytic model as a function of the 2-dimensional projected density with the photometric redshift error at each redshift. Solid line shows the fraction at $z \sim 0.9$, while dashed line represents that at $z \sim 1.2$. Left panel shows the fraction of model galaxies with $EW_0([\text{O II}]) > 12 \text{ \AA}$, while right panel shows the fraction of those with $EW_0([\text{O II}]) > 36 \text{ \AA}$.

the fraction of H α emitters with $EW_{\text{obs}}(\text{H}\alpha) > 50 \text{ \AA}$ is $\sim 30\%$ almost independent of the local density in relatively low-density environments of their $\Sigma_c < 10 \text{ Mpc}^{-2}$. On the other hand, the fraction rapidly decreases with increasing the local density in higher-density environments. If the environments we investigated are mainly field environments, our result at $z \sim 0.9$ is consistent with that in Sobral et al. (2011). In this study, we also found that the evolution of the fraction of [O II] emitters between $z \sim 1.2$ and $z \sim 0.9$ is also independent of the galaxy environment in the range of the environment we investigated. Sobral et al. (2011) suggested that the star formation in the field environment is dominated by normal (non-interacting) galaxies, while the star formation in the rich group and cluster environment is dominated by the potential mergers (e.g., Ideue et al. 2012; Hayashi et al. 2010). If this is the case, the galaxy interactions might not play an important role in the star formation activity of most field galaxies. As a result, the evolution of star formation activity in these galaxies between $z \sim 1.2$ and $z \sim 0.9$ does not depend on the galaxy environment, but might simply be related with physical properties of each galaxy such as gas mass fraction.

4.2. Evolution of the fraction of [O II] emitters between $z \sim 1.2$ and $z \sim 0.9$

In this section, we discuss the strength of the evolution in the fraction of [O II] emitters from $\sim 60\%$ at $z \sim 1.2$ to $\sim 30\%$ at $z \sim 0.9$. At first, we examined how the local density for each galaxy evolves between $z \sim 1.2$ and $z \sim 0.9$ by using the same semi-analytic model as in Section 3.3, since the strong evolution of the density could make the comparison between the different redshifts more complicated (e.g., Poggianti et al. 2010). Figure 10 shows the comparisons of the local density between the redshifts for the same model galaxies for the Sample A and Sample B. For model galaxies at $z \sim 1.2$, we similarly calculated the 3-dimensional density and the 2-dimensional projected density including the random offsets due to the photo- z error at $z \sim 1.2$.

Note that the average number densities of galaxies at $z \sim 0.9$ are different between the both samples by a factor of ~ 2 . It is seen from the upper panels of the figure that the evolution of the true 3-dimensional density is relatively small (a factor of $\lesssim 2$) for most model galaxies except for the high density region. The projected density also mildly evolves at $0.3 \text{ Mpc}^{-2} \leq \Sigma_{10\text{th}} \leq 10 \text{ Mpc}^{-2}$ especially for the Sample B. By combining this with the lack of the environmental dependence at the both redshifts, we infer that the change in the local density probably does not strongly affect the evolution of the fraction of [O II] emitters in the range of the density we investigated. Therefore we can fairly compare the fractions of [O II] emitters at the same range of the local density between $z \sim 1.2$ and $z \sim 0.9$.

In Figure 11, we plot the evolution of the fraction of [O II] emitters between $z \sim 0.9$ and $z \sim 1.2$ predicted by the semi-analytic model. The strength of the evolution in the model does not seem to be affected by the criterion of $EW_0([\text{O II}])$, and it could be slightly large at $\Sigma_{10\text{th}} \sim 3\text{--}10 \text{ Mpc}^{-2}$. The observed strength of the evolution seen in Figure 3 is larger than that in the model.

We next consider the evolution of the $EW_0([\text{O II}])$ distribution. Figure 12 shows a comparison of the observed $EW_0([\text{O II}])$ distribution between the $z \sim 0.9$ and $z \sim 1.2$ samples. The $EW_0([\text{O II}])$ for each [O II] emitter is calculated from the narrow-band excess ($\text{NB711} - ri'$). In Figure 12, the fraction of galaxies with $EW_0([\text{O II}]) > 12 \text{ \AA}$ at $z \sim 0.9$ is lower than that at $z \sim 1.2$ as expected from Figure 3. If we simply assume the $EW_0([\text{O II}])$ of all star-forming galaxies decreases by the same factor from $z \sim 1.2$ and $z \sim 0.9$, the observed $EW_0([\text{O II}])$ distributions suggest that the $EW_0([\text{O II}])$ needs to decrease by a factor of $1.75^{+0.55}_{-0.35}$ in this redshift interval in order to reproduce the fraction of [O II] emitters with $EW_0([\text{O II}]) \geq 12 \text{ \AA}$ at $z \sim 0.9$ ($\sim 0.3 \pm 0.1$).

We here try to interpret the $EW_0([\text{O II}])$ evolution as the evolution of star formation activity in galaxies. Figure 13 compares [O II] LFs between $z \sim 0.9$ and $z \sim 1.2$

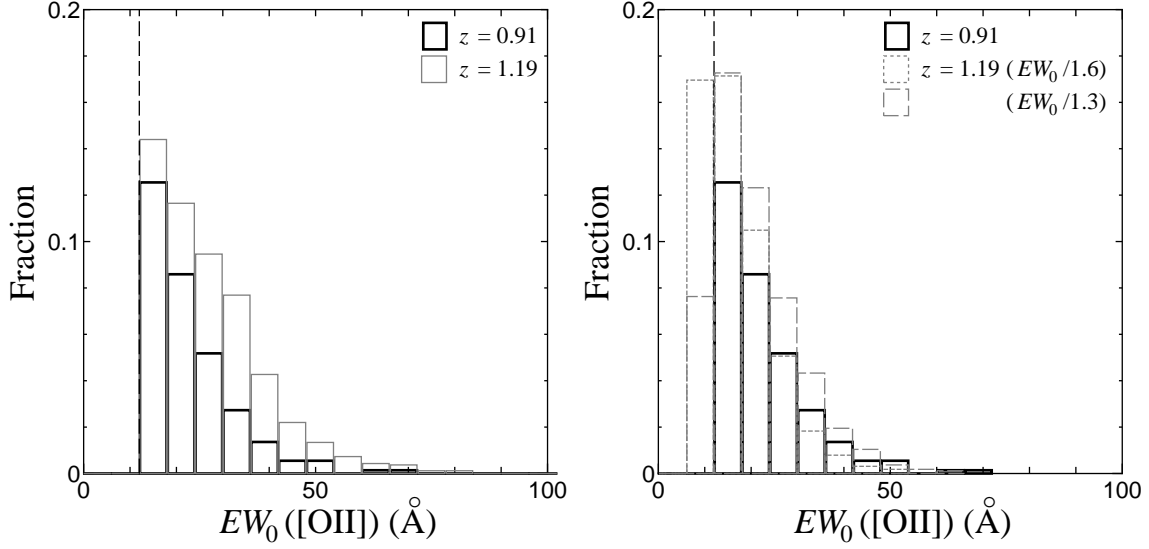


FIG. 12.— **left)** Comparison of the normalized differential distributions of $EW_0([\text{O II}])$ between $z \sim 0.9$ and $z \sim 1.2$. black and grey histograms show that for galaxies at $z \sim 0.9$ and $z \sim 1.2$, respectively. Vertical dashed line shows the equivalent width limit of $EW_0([\text{O II}]) = 12 \text{ \AA}$ for our [O II] emitter selection. Note that only galaxies classified as [O II] emitters are plotted, while the calculation of the normalization constant takes account of all galaxies including objects which do not satisfy the selection criteria for the [O II] emitter. **right)** The same as the left panel, but the observed $EW_0([\text{O II}])$ for [O II] emitters at $z \sim 1.2$ is divided by a factor of 1.3 and 1.6 (short- and long-dashed histograms). A decrease of a factor of 1.3–1.6 in $EW_0([\text{O II}])$ from $z \sim 1.2$ to $z \sim 0.9$ is expected from the simple model where SFRs of star-forming galaxies decreases by a factor of 2 in the redshift interval (see text).

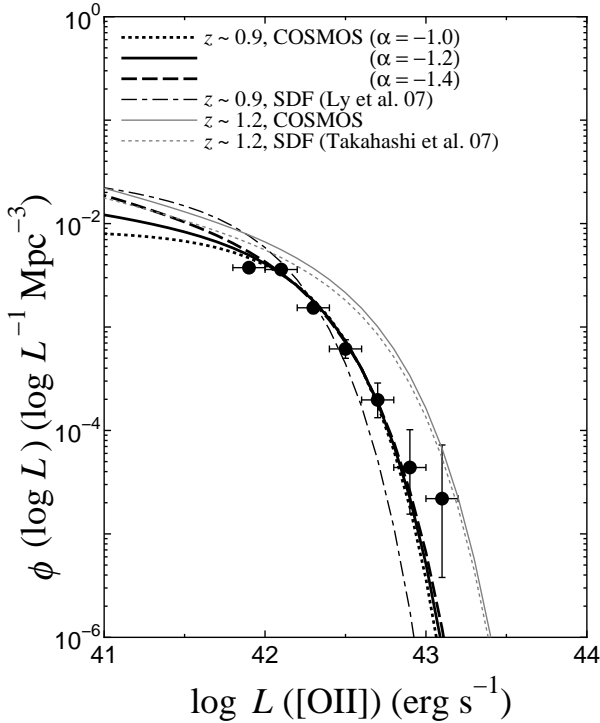


FIG. 13.— The [O II] luminosity function for [O II] emitters at $z \sim 0.9$ and $z \sim 1.2$. The solid circles show the result for our [O II] emitter sample at $z \sim 0.9$ in the COSMOS field. The thick dotted, solid, and dashed lines represent the best-fit Schechter functions for $\alpha = -1.0$, -1.2 , and -1.4 , respectively. Thin dashed-dotted line shows [O II] LF for [O II] emitters at $z \sim 0.9$ in the Subaru Deep Field from Ly et al. (2007). Thin solid line represents the result at $z \sim 1.2$ in the COSMOS field updated from Takahashi et al. (2007) with the newest version of the COSMOS photometric redshift catalog. Thin dotted lines show [O II] LF at $z \sim 1.2$ in the Subaru Deep Field from Takahashi et al. (2007).

in the COSMOS field and the Subaru Deep Field (SDF). The [O II] LFs in the COSMOS field are derived from our samples at $z \sim 0.9$ and $z \sim 1.2$ (Appendix A), and those in the SDF are the results by Ly et al. (2007). It is seen that the characteristic luminosity decreases by a factor of ~ 2 from $\log L_* \sim 42.5$ at $z \sim 1.2$ to $\log L_* \sim 42.2$ at $z \sim 0.9$ in the both fields, while the normalization shows no significant evolution. If we assume that there is no strong evolution in the average metallicity of galaxies between $z \sim 1.2$ and $z \sim 0.9$, this luminosity evolution reflects the decrease of the star formation activity in galaxies. Many previous studies of the evolution of the cosmic SFR density also suggest that the star formation activity in the universe decreases by a factor of ~ 2 from $z \sim 1.2$ to $z \sim 0.9$ on average (e.g., Hopkins & Beacom 2006; Sobral et al. 2012). Then we calculate the evolution in the $EW_0([\text{O II}])$ for the case that the star formation rate decreases by a factor of 2 in the redshift interval. The [O II] line luminosity is simply expected to decrease by the same factor as the SFR, if we ignore the metallicity/dust extinction evolution. If we assume exponentially decaying star formation histories (i.e., $\text{SFR} \propto \exp(-\text{age}/\tau)$) between $z \sim 1.2$ and $z \sim 0.9$ for simplicity, the evolution of factor of ~ 2 in the SFR which is expected from the [O II] luminosity function at $z \sim 1.2$ and $z \sim 0.9$ corresponds to the star formation timescale of $\tau = 1.2\text{--}1.8$ Gyr. In this case, the continuum luminosity at the rest-frame 3727 \AA is expected to decrease by a factor of ~ 1.5 . This is also consistent with the evolution of the characteristic magnitude of the rest-frame 3500 \AA LF (0.4 mag) mentioned in Section 2.1. Therefore, we can expect that the $EW_0([\text{O II}])$ decreases by a factor of 1.3–1.6 between $z \sim 1.2$ and $z \sim 0.9$, taking account of the possible effect of the Balmer break on the measurement of the narrow-band excess (NB711 – ri'). This is roughly consistent with the evolution of the

$EW_0([\text{O II}])$ expected from the evolution in the fraction of $[\text{O II}]$ emitters ($1.75_{-0.35}^{+0.55}$). In the right panel of Figure 12, we compare the observed $EW_0([\text{O II}])$ distribution at $z \sim 0.9$ with the simulated distributions which are calculated by dividing the $EW_0([\text{O II}])$ at $z \sim 1.2$ by a factor of 1.3 and 1.6. The agreement of the $EW_0([\text{O II}])$ distribution is relatively good especially in the case that the $EW_0([\text{O II}])$ decreases by a factor of 1.6, although the observed $EW_0([\text{O II}])$ at $z \sim 0.9$ could be slightly lower than those predicted from the evolution of the star formation activity. Thus, the decrease of the fraction of $[\text{O II}]$ emitters from $z \sim 1.2$ to $z \sim 0.9$ seems to be explained mainly by the decrease of the overall star formation activity in the universe, while the additional offset seen in the right panel of Figure 12 might be explained by the evolution of the gas metallicity and/or dust extinction in star-forming galaxies.

5. SUMMARY

We investigated the fraction of $[\text{O II}]$ emitters in the photo- z selected galaxies at $z \sim 0.9$ as a function of the local galaxy density in the COSMOS field. $[\text{O II}]$ emitters are selected by the narrow-band excess technique with the NB711-band data taken with Subaru/Suprime-Cam. We used the magnitude limits and selection criteria for $[\text{O II}]$ emitters which are consistent with our previous study at $z \sim 1.2$ in order to make a direct comparison between $z \sim 0.9$ and $z \sim 1.2$. Our final sample consists of 614 (291) photo- z selected galaxies with $M_{U3500} < -19.31$ ($M_{U3500} < -19.71$) at $z = 0.901 - 0.920$, which includes 195 (95) $[\text{O II}]$ emitters. Our main results are as follows.

- The fraction of $[\text{O II}]$ emitters at $z \sim 0.9$ is nearly constant (~ 0.3) at $0.3 \text{ Mpc}^{-2} < \Sigma_{10\text{th}} < 10 \text{ Mpc}^{-2}$. The flat distribution holds, even if we use the magnitude limit for which the luminosity evolution of galaxies is taken into account. No significant environmental dependence is similar with the result in our previous study at $z \sim 1.2$.
- The fraction of $[\text{O II}]$ emitters decreases from ~ 0.6 at $z \sim 1.2$ to ~ 0.3 at $z \sim 0.9$ in all environment we investigated.
- Instead of $[\text{O II}]$ emitters, we used galaxies with blue rest-frame colors of $NUV - R < 2$ at $0.91 - 0.023 \leq z_{\text{phot}} \leq 0.91 + 0.023$ as the star-forming

population in order to measure both the fraction of star-forming galaxies and local galaxy density from the same sample. The fraction of blue galaxies with $NUV - R < 2$ also does not significantly depend on the local density.

- We checked the effects of the projection over the redshift slice and the photometric redshift error on our density measurement, using the semi-analytic model by Font et al. (2008). Although these effects seem to smear out very high and low density regions in some degree, we confirmed that the fraction of $[\text{O II}]$ emitters clearly depends on the projected density in the simulation, which is different from the observed results.
- Most of $[\text{O II}]$ emitters have relatively small stellar mass of $M_{\text{star}} < 10^{10} M_{\odot}$, and the overlap between $[\text{O II}]$ emitters and bright $24\mu\text{m}$ sources with $f_{24\mu\text{m}} \gtrsim 150\text{--}200 \mu\text{Jy}$ is relatively small. The $[\text{O II}]$ emitter selection seems to miss massive dusty star-forming galaxies. Such a selection bias might cause the different behaviors in the SFR-density relation among studies with the different SFR indicators.
- If we simply assume SFRs of star-forming galaxies decrease by a factor of 2 from $z \sim 1.2$ to $z \sim 0.9$, which is expected from the evolution of the $[\text{O II}]$ luminosity function and cosmic SFR density in the redshift interval, the expected evolution of the $EW_0([\text{O II}])$ is roughly consistent with the observed $EW_0([\text{O II}])$ distributions at $z \sim 1.2$ and $z \sim 0.9$. Therefore the decrease of the fraction of $[\text{O II}]$ emitters from $z \sim 1.2$ to $z \sim 0.9$ seems to be explained mainly by the decrease of the overall star formation activity in the universe.

We would like to thank the referee for invaluable suggestions and comments. The HST COSMOS Treasury program was supported through NASA grant HST-GO-09822. We greatly acknowledge the contributions of the entire COSMOS collaboration consisting of more than 70 scientists. This work was financially supported in part by the Japan Society for the Promotion of Science (Nos. 17253001, 19340046, 23244031, 23654068, and 23740152).

APPENDIX

LUMINOSITY FUNCTION OF $[\text{O II}]$ EMITTERS AT $Z \sim 1.2$ IN THE COSMOS FIELD

In this Appendix, we describe the derivation of the $[\text{O II}]$ luminosity function at $z \sim 0.9$ in the COSMOS field. To derive the total $[\text{O II}]$ flux, we have used the total flux density of r' , i' (or i^*), and NB711. The flux of $[\text{O II}]$ emission line is given by

$$f_{[\text{O II}]} = \Delta\text{NB} \frac{f_{\text{NB}} - f_{ri}}{1 - 0.68(\Delta\text{NB}/\Delta i')} \quad (\text{A1})$$

where f_{NB} is the total flux density of NB711, f_{ri} is the ri continuum flux density, ΔNB and $\Delta i'$ are the effective bandwidth of the NB711 and i' filters, respectively: $\Delta\text{NB711} = 72.5 \text{ \AA}$ and $\Delta i' = 1489.4 \text{ \AA}$. Since the flux of the $[\text{O II}]$ emission line is affected by the dust obscuration, it is necessary to correct the extinction effect. Here, we apply a constant extinction of $A_{[\text{O II}]} = 1.87 \text{ mag}$, which corresponds to $A_{\text{H}\alpha} = 1 \text{ mag}$, following previous studies (Hopkins 2004; Takahashi et al. 2007; Sobral et al. 2012). We also apply the filter transmission effect since the actual NB711 filter transmission is not rectangular. We adopt a factor of 1.24 following Shioya et al. (2009).

TABLE 2
BEST-FIT SCHECHTER PARAMETERS FOR THE [O II] LUMINOSITY FUNCTION AT $z \sim 0.9$ IN THE COSMOS FIELD.

α	$\log L_*$	$\log \phi_*$
-1.00	42.11 ± 0.03	-2.43 ± 0.05
-1.20	42.16 ± 0.04	-2.48 ± 0.06
-1.40	42.21 ± 0.04	$-2.55^{+0.07}_{-0.06}$

Then the [O II] flux is given by

$$f_{\text{cor}}([\text{O II}]) = f_{[\text{O II}]} \times 10^{0.4A_{[\text{O II}]}} \times 1.24, \quad (\text{A2})$$

and the [O II] luminosity is estimated by

$$L([\text{O II}]) = 4\pi d_L^2 f_{\text{cor}}([\text{O II}]) \quad (\text{A3})$$

where d_L is the luminosity distance: $d_L = 5883$ Mpc.

The [O II] luminosity function (LF) is constructed by the following formula,

$$\Phi(\log L_i) = \frac{1}{\Delta \log L} \sum_j \frac{1}{V_j}, \quad (\text{A4})$$

with $|\log L_j - \log L_i| < \frac{1}{2} \Delta \log L$, where $\Delta \log L$ is the logarithmic bin size and V_j is the volume covered by the filter. Here we use $\Delta \log L = 0.2$, and $V_j = 2.28 \times 10^5$ Mpc³. We show the [O II] LF in Figure 13.

We fit the [O II] LF with the Schechter function (Schechter 1976),

$$\Phi(L)dL = \frac{\phi_*}{L_*} \left(\frac{L}{L_*} \right)^\alpha \exp\left(-\frac{L}{L_*}\right) dL, \quad (\text{A5})$$

by the STY method (Sandage et al. 1979). Before fitting the [O II] LF, we estimate the lower and upper limiting luminosities (L_{low} and L_{up}) that evaluate whether the sample is complete or not. Using the observed limiting magnitudes of ri and NB711, we obtain $\log L_{\text{low}} = 41.83$ erg s⁻¹. On the other hand, the saturation magnitude of r' gives the upper limiting luminosity of $\log L_{\text{up}} = 43.65$ erg s⁻¹. Since it is difficult to estimate the power index α accurately because of incompleteness at the faint end, we show our results for the following three cases, $\alpha = -1.0, -1.2$, and -1.4 in Table 2.

REFERENCES

- Balogh, M., Eke, V., Miller, C., et al. 2004, MNRAS, 348, 1355
 Bamford, S. P., Nichol, R. C., Baldry, I. K., et al. 2009, MNRAS, 393, 1324
 Blanton, M. R., Eisenstein, D., Hogg, D. W., & Zehavi, I. 2006, ApJ, 645, 977
 Bower, R. G., Benson, A. J., Malbon, R., et al. 2006, MNRAS, 370, 645
 Bruzual, G., & Charlot, S. 2003, MNRAS, 344, 1000
 Bundy, K., Scarlata, C., Carollo, C. M., et al. 2010, ApJ, 719, 1969
 Capak, P., Aussel, H., Ajiki, M., et al. 2007, ApJS, 172, 99
 Chabrier, G. 2003, PASP, 115, 763
 Cooper, M. C., Newman, J. A., Weiner, B. J., et al. 2008, MNRAS, 383, 1058
 Dressler, A. 1980, ApJ, 236, 351
 Elbaz, D., Daddi, E., Le Borgne, D., et al. 2007, A&A, 468, 33
 Font, A. S., Bower, R. G., McCarthy, I. G., et al. 2008, MNRAS, 389, 1619
 Gómez, P. L., Nichol, R. C., Miller, C. J., et al. 2003, ApJ, 584, 210
 Goto, T., Yamauchi, C., Fujita, Y., et al. 2003, MNRAS, 346, 601
 Hayashi, M., Kodama, T., Koyama, Y., et al. 2010, MNRAS, 402, 1980
 Hopkins, A. M. 2004, ApJ, 615, 209
 Hopkins, A. M., & Beacom, J. F. 2006, ApJ, 651, 142
 Ideue, Y., Nagao, T., Taniguchi, Y., et al. 2009, ApJ, 700, 971
 Ideue, Y., Taniguchi, Y., Nagao, T., et al. 2012, ApJ, 747, 42
 Ilbert, O., Capak, P., Salvato, M., et al. 2009, ApJ, 690, 1236
 Ilbert, O., Salvato, M., Le Floch, E., et al. 2010, ApJ, 709, 644
 Kajisawa, M., Ichikawa, T., Yamada, T., et al. 2010, ApJ, 723, 129
 Kauffmann, G., White, S. D. M., Heckman, T. M., et al. 2004, MNRAS, 353, 713
 Koyama, Y., Kodama, T., Shimasaku, K., et al. 2010, MNRAS, 403, 1611
 Lacy, M., Storrer-Lombardi, L. J., Sajina, A., et al. 2004, ApJS, 154, 166
 Lilly, S. J., Le Brun, V., Maier, C., et al. 2009, ApJS, 184, 218
 Lilly, S. J., Le Fèvre, O., Renzini, A., et al. 2007, ApJS, 172, 70
 Ly, C., Malkan, M. A., Kashikawa, N., et al. 2007, ApJ, 657, 738
 Patel, S. G., Holden, B. P., Kelson, D. D., Illingworth, G. D., & Franx, M. 2009, ApJ, 705, L67
 Patel, S. G., Kelson, D. D., Holden, B. P., Franx, M., & Illingworth, G. D. 2011, ApJ, 735, 53
 Poggianti, B. M., Desai, V., Finn, R., et al. 2008, ApJ, 684, 888
 Poggianti, B. M., De Lucia, G., Varela, J., et al. 2010, MNRAS, 405, 995
 Sandage, A., Tammann, G. A., & Yahil, A. 1979, ApJ, 232, 352
 Sanders, D. B., Salvato, M., Aussel, H., et al. 2007, ApJS, 172, 86
 Schechter, P. 1976, ApJ, 203, 297
 Scoville, N., Aussel, H., Brusca, M., et al. 2007, ApJS, 172, 1
 Shioya, Y., Taniguchi, Y., Sasaki, S. S., et al. 2008, ApJS, 175, 128
 Shioya, Y., Taniguchi, Y., Sasaki, S. S., et al. 2009, ApJ, 696, 546
 Sobral, D., Best, P. N., Smail, I., et al. 2011, MNRAS, 411, 675
 Sobral, D., Best, P. N., Matsuda, Y., et al. 2012, MNRAS, 420, 1926
 Springel, V., White, S. D. M., Jenkins, A., et al. 2005, Nature, 435, 629
 Stern, D., Eisenhardt, P., Gorjian, V., et al. 2005, ApJ, 631, 163
 Takahashi, M. I., Shioya, Y., Taniguchi, Y., et al. 2007, ApJS, 172, 456
 Tanaka, M., Goto, T., Okamura, S., Shimasaku, K., & Brinkmann, J. 2004, AJ, 128, 2677
 Taniguchi, Y., Scoville, N., Murayama, T., et al. 2007, ApJS, 172, 9

- Tran, K.-V. H., Papovich, C., Saintonge, A., et al. 2010, *ApJ*, 719, L126
- Westra, E., Geller, M. J., Kurtz, M. J., Fabricant, D. G., & Dell'Antonio, I. 2010, *ApJ*, 708, 534